# Effect of potassium or yttrium introduction in Yb3+-doped germano-gallate glasses on the structural, luminescence properties and fiber processing

Rayan Zaiter, Téa Skopak, Yannick Ledemi, Marc Dussauze, Frédéric Adamietz, Evelyne Fargin, Younes Messaddeq, Sylvain Danto, Thierry Cardinal

# Effect of potassium or yttrium introduction in $Yb^{3+}$-doped germano-gallate glasses on the structural, luminescence properties and fiber processing

R. Zaiter[1*], T. Skopak[1,2], Y. Ledemi[2], M. Dussauze[3], F. Adamietz[3], E. Fargin[1], Y. Messaddeq[2], S. Danto[1], T. Cardinal[1]

[1] Institut de Chimie de la Matière Condensée de Bordeaux, ICMCB-CNRS, Université de Bordeaux, Bordeaux, France

[2] Centre d'Optique, Photonique et Laser, COPL, Université Laval, Québec, QC, Canada

[3] Institut des Sciences Moléculaires, ISM, Université de Bordeaux, Bordeaux, France

*Corresponding author: rayan.zaiter@icmcb.cnrs.fr

## Abstract

Here we report on the effect of potassium or yttrium on the luminescence spectroscopic properties of $Yb^{3+}$-doped germano-gallate glasses as well as the ability to shape them into optical fibers with the objective of using such glasses to produce near-infrared optical gain medium. Two ytterbium-doped germano-gallate glass systems, $(100\text{-}x)$ $(28Ga_2O_3 – 37GeO_2 – 23BaO – 12K_2O) – xYb_2O_3$ ($x$ = 0, 0.5 and 3 mol.%) and $29.6Ga_2O_3 – 39.1GeO_2 – 24.3BaO – 7$ ($yY_2O_3 – zYb_2O_3$) ($y$ = 6.5, 4, 0 and $z$ = 0.5, 3, 7 mol% respectively) have been prepared and the systematic investigation of their thermal, structural, optical and spectroscopic properties have been carried out. The increase in ytterbium oxide content leads to an increase of the glass transition temperature, crystallization temperature and the density of the glasses, as well as induces a red-shift of the cut-off wavelength. Raman spectroscopy analysis shows that both ytterbium oxide addition and potassium substitution by yttrium modify the 3D interconnected germano-gallate glass network. Lifetime diminishes with the increase of $Yb^{3+}$ concentration but remains higher in the yttrium-containing glasses. We demonstrate that the production of crystal-free light guiding fibers via the preform-to-fiber approach becomes possible only in the yttrium-containing glass system. Cut-back optical attenuation measurements of the produced fibers show minimum losses of 3.3 dB/m at 1310 nm.

Keywords: germano-gallate glasses, infrared, Raman spectroscopy, luminescence, life-time, fibers

## 1. Introduction

Ytterbium-doped glasses form a strategic class of active mediums for the development of numerous laser emitting devices in the near-infrared (NIR) range [1], [2]. Trivalent ytterbium ions own a simple energy level scheme, with the $^2F_{7/2}$ being the ground state and the $^2F_{5/2}$ being the excited state. It has a high cross-section absorption band located at about 975 nm, allowing efficient pumping by commercially available semi-conductor diodes. $Yb^{3+}$ ions offer a broad emission band centered at 1030 nm with a longer fluorescence lifetime and are in addition excellent energy transfer sensitizers for other lanthanide elements for up conversion lasers [3]. Due to its technological interest for all-solid-state lasers, the NIR emission of the ytterbium ion doping has been explored in numerous crystals [4]–[6], but also in glasses and glass-ceramics systems such as in silicates [1], [2], [7], phosphates [8], [9], tellurites [10], oxyborates [11] or heavy metal oxides [12]–[15]. Among glasses, $Yb^{3+}$-doped phosphate-based materials led to the most advanced developments as high-power fiber lasers [16]–[18].

Germano-gallate glasses are optical materials transparent up to ~5.5 µm in the mid-IR, yet with higher glass transition temperature and superior mechanical properties as compared to other mid-IR glasses (e.g. fluoride, tellurite, chalcogenides) [19]. Due to the much better glass-forming ability of $GeO_2$ compared to the $Ga_2O_3$ (known as glass network intermediate), most studies performed to date on these materials have relied on vitreous compositions made of $GeO_2$ as main constituent, usually well above 50 mol.%. However, gallate glasses have attracted recent attention. We have reported on the structure-properties relationship in gallium-rich glass systems $GaO_{3/2}$ – $GeO_2$ – $NaO_{1/2}$ [20], $GaO_{3/2}$ – $LaO_{3/2}$ – $KO_{1/2}$ [21], $GaO_{3/2}$ – $GeO_2$ – BaO – $KO_{1/2}$ [22], [23], $GaO_{3/2}$ – $GeO_2$ – BaO – $LaO_{3/2}$ – $YO_{3/2}$ [23] and $GaO_{3/2}$ – $GeO_2$ – BaO – $LaO_{3/2}$ [24].

Following a similar approach, here we report on the physicochemical, structural and spectroscopic properties of $GaO_{3/2}$-rich germano-gallate glasses doped with ytterbium oxide in the system (100-$x$) ($28Ga_2O_3$ – $37GeO_2$ – 23BaO – $12K_2O$) – $xYb_2O_3$ ($x$ = 0 to 7 mol.%). The host glass matrix was selected due to its wide optical transparency, extending from ~280 nm in the UV up to ~5.5 µm in the mid-IR, high refractive index (up to 1.7), high glass transition temperature ($T_g$ ~700 °C) and high damage threshold [22], [23]. However, because of surface crystallization, the fiber drawing ability of these materials could be accessed only from an open-crucible route [22], [23]. Recently, one demonstrated that the introduction of rare earth ions in germano-gallate glasses can circumvent this detrimental glass crystallization and enables the preform-to-fiber drawing [23]. Therefore, we report also on the synthesis and characterization of $29.6Ga_2O_3$ – $39.1GeO_2$ – 24.3BaO – 7 ($yY_2O_3$ – $zYb_2O_3$) ($y$ = 6.5, 4, 0 and $z$ = 0.5, 3, 7 respectively) glasses, in order to elucidate the relation between the structure and properties. To this end, luminescent and spectroscopic properties (absorption and emission cross-section, lifetime decay) of the glasses have been explored in order to evaluate the difference of performance of $Yb^{3+}$ in potassium- and yttrium-containing glasses.

## 2. Experimental details

### *2.1. Glass preparation*

Glasses were prepared by conventional melt-quenching technique from gallium oxide $Ga_2O_3$ (99.9% from Strem Chemical), germanium oxide $GeO_2$ (99.999% from Strem Chemical), barium carbonate $BaCO_3$ (99% from ACS Merck), potassium carbonate $K_2CO_3$ (99% from Sigma Aldrich), yttrium oxide $Y_2O_3$ (99.999% from Strem Chemical) and ytterbium oxide $Yb_2O_3$ (99.99% from Alfa Aesar). The powder precursors were mixed and placed in a platinum crucible for a pre-sintering treatment at 1200 °C for 2 hours and then melted under ambient atmosphere at 1400-1600 °C for 4 hours. The melted glass was then quenched in the ambient air, grounded and melted a second time in order to increase its homogeneity. The resulting glass was annealed at $T_g$-40 °C for 4 hours and slowly cooled down to room temperature. Transparent, bubbles-free glass chunks were obtained. Then the samples were cut and polished with parallel faces for further characterizations.

### *2.2. Thermal, physical and structural characterization*

The vitreous state of the samples and the absence of crystallites related to the high content of $Yb_2O_3$ were confirmed by powder X-Ray Diffraction (XRD) patterns which were collected on a PANalitycal X'pert PRO MPD diffractometer in Bragg-Brentano θ-θ geometry equipped with a secondary monochromator and X'Celerator multi-strip detector. Thermal properties which include the transition temperature ($T_g$) and the onset of crystallization ($T_x$) were measured on a Netzsch DSC Pegasus 404 PC apparatus with glass chunks in a Pt pan at a heating rate of 10 °C/min up to 1000 °C with a precision of ±3 °C. The density $\rho$ was measured by Archimede's method by immerging a glass chunk in diethyl phthalate at room temperature on a Precisa XT 220A weighing scale with an estimated error of ±0.01 g/cm$^3$.

The transmission spectra in the UV-Visible-NIR and the IR range were respectively obtained from Agilent Cary 5000 (UV-Visible) and Bruker Equinox 55 (FTIR). The multiphonon cut-off ($\lambda_{IR}$) and the short wavelength cut-off ($\lambda_{UV}$). The linear refractive index for the potassium-containing glasses was measured by prism coupling technique with a Metricon M2010 apparatus at 972 nm. The refractive index for the yttrium-containing glasses was determined by measuring the Brewster angle at 935 nm with an estimated error of ±0.005. The Raman spectra were obtained using a Horiba Jobin-Yvon XploRA Raman spectrometer with a spectral resolution of 2 cm$^{-1}$, equipped with a 532 nm laser and a confocal microscope (50×). The obtained spectra were normalized to area.

The photoluminescence emission spectra have been recorded on powdered samples with a Horiba Jobin Yvon Nanolog spectrofluorimeter by using a Xenon lamp, a double excitation monochromator, an iHR320 emission monochromator and an Hamamatsu PMT detector operating from 850 to 1700 nm. Infrared lifetime measurements were performed with a digital oscilloscope (LeCroy Waverunner LT

342) equipped with a germanium AD403HS detector coupled to a HR640 monochormator (Horiba Jobin-Yvon). Self-made Labview program was used for piloting the experiments.

### *2.3. Glass preform preparation, fiber drawing and optical loss measurements*

Initially, around 35 grams mono-index glass rod was prepared by the melt-quenching method. The preform with dimensions of 1 cm in diameter and 7 cm in length was then annealed at $T_g$-40 °C for 2 hours. Afterwards, the preform was drawn using a dedicated optical fiber drawing towers equipped with an annular resistive furnace having a sharp temperature profile. The heating chamber was kept under continuous oxygen gas flow (3 $L.min^{-1}$). The preform was fed into the furnace and the temperature was gradually raised up to ~750 °C using a heating rate of 20 °C/min, then to ~950 °C with a heating rate of 10°C/min to soften the bottom-section of the preform.

Optical fiber attenuation was recorded using the cut-back method. The measurements were performed using the 1310 nm laser diode module (from Power Technology) and thermopile detector (XLP12-3S-H2-D0 from Gentec). The quality of cleaving was systematically inspected with a microscope objective and special attention was paid to limit the fiber curvature during the measurement.

## 3. Results and discussion

### *3.1. Glass compositions and physicochemical properties*

Glass compositions were prepared following the composition law (100-$x$) ($28Ga_2O_3 – 37GeO_2 – 23BaO – 12K_2O$) – $xYb_2O_3$ with $x$ = 0, 0.5 and 3 mol.% (samples labelled as GGBK-Yb$x$). Because of surface crystallization and the formation of zeolite-type crystalline structures, access to fibers in this system can only be approached from the melt by the open-crucible route [22], [23]. As supported by earlier observations [23], substitution of the potassium with yttrium was investigated in order to mitigate surface crystallization. Following, the glasses in the system $29.6Ga_2O_3 – 39.1GeO_2 – 24.3BaO – 7$ ($yY_2O_3 – zYb_2O_3$) ($y$ = 6.5, 4, 0 and $z$ = 0.5, 3, 7 mol.% respectively) were synthesized while keeping the same ratio of $GaO_{3/2}/GeO_2$ which is equal to 1.5. The Table 1 summarizes the investigated nominal glass compositions in mole percent and cationic percent of oxide precursors and the corresponding $Yb^{3+}$ ion concentration. The cationic percent highlights the high content of gallium cations in the selected matrix. Bubble-free homogeneous glass samples were obtained as can be seen in Figure 1.

**Table 1.** Nominal GGBK-Yb and GGBY-Yb glass compositions (in mol.% and cationic mol.%) studied in this work and $Yb^{3+}$ ions concentration.

| | Nominal compositions (mol.%) | | | | | | Nominal compositions (cat.%) | | | | | | $Yb^{3+}$ ions/$cm^3$ |
|---|---|---|---|---|---|---|---|---|---|---|---|---|---|
| **Sample** | $Ga_2O_3$ | $GeO_2$ | BaO | $K_2O$ | $Y_2O_3$ | $Yb_2O_3$ | $GaO_{3/2}$ | $GeO_2$ | BaO | $KO_{1/2}$ | $YO_{3/2}$ | $YbO_{3/2}$ | |
| GGBK-Yb0 | 28.0 | 37.0 | 23.0 | 12.0 | - | 0.0 | 40.0 | 26.4 | 16.4 | 17.1 | - | 0.0 | 0 |
| GGBK-Yb0.5 | 27.9 | 36.8 | 22.9 | 11.9 | - | 0.5 | 39.8 | 26.2 | 16.3 | 17.0 | - | 0.7 | $1.89\ 10^{20}$ |
| GGBK-Yb3 | 27.2 | 35.9 | 22.3 | 11.6 | - | 3.0 | 38.4 | 25.3 | 15.7 | 16.4 | - | 4.2 | $1.13\ 10^{21}$ |

| | | | | | | | | | | | | | |
|---|---|---|---|---|---|---|---|---|---|---|---|---|---|
| GGBY-Yb0.5 | 29.6 | 39.1 | 24.3 | - | 6.5 | 0.5 | 43.3 | 28.6 | 17.8 | - | 9.5 | 0.7 | 1.94 $10^{20}$ |
| GGBY-Yb3 | 29.6 | 39.1 | 24.3 | - | 4.0 | 3.0 | 43.3 | 28.6 | 17.8 | - | 5.9 | 4.4 | 1.19 $10^{21}$ |
| GGB-Yb7 | 29.6 | 39.1 | 24.3 | - | - | 7.0 | 43.3 | 28.6 | 17.8 | - | - | 10.2 | 2.80 $10^{21}$ |

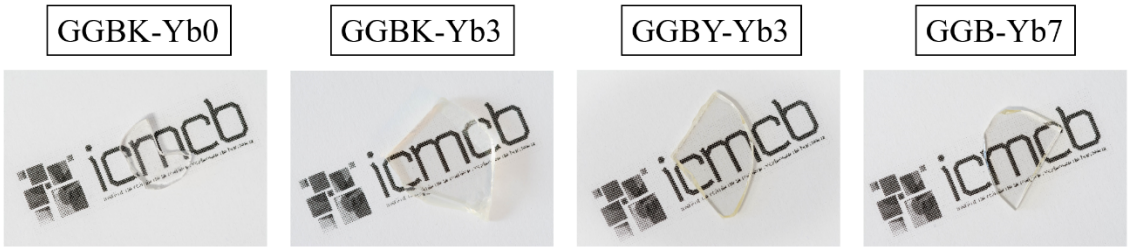


**Figure 1.** Photographs of GGBK-Yb0, GGBK-Yb3, GGBY-Yb3 and GGB-Yb7 glass samples after cutting and polishing.

The main physicochemical properties of the GGBK-Yb and GGBY-Yb glasses are reported in Table 2 ($T_g$: glass transition temperature, $T_x$: onset of crystallization temperature, $\Delta T = T_x - T_g$, thermal stability against crystallization criterion, $\rho$: density, $\lambda_{UV}$: short wavelength cut-off and $n$: refractive index at 972 nm or 935 nm.

**Table 2.** Physicochemical properties of the GGBK-Yb and GGBY-Yb glasses: glass transition ($T_g$) and onset of crystallization ($T_x$) temperatures, thermal stability against crystallization ($\Delta T$), glass density ($\rho$), short wavelength cut-off ($\lambda_{UV}$) and refractive index at 972 nm or 935 nm ($n$).

| **Sample** | $T_g$ **(±3°C)** | $T_x$ **(±3°C)** | $\Delta T$ **(±3°C)** | $\rho$ **(±0.01 g.cm$^{-3}$)** | $\lambda_{UV}$ **(± 1nm)** | $n$ **(±0.005)** |
|---|---|---|---|---|---|---|
| GGBK-Yb0 | 675 | 840 | 165 | 4.30 | 281 | 1.675* |
| GGBK-Yb0.5 | 688 | 839 | 151 | 4.36 | 286 | 1.678* |
| GGBK-Yb3 | 708 | 876 | 168 | 4.54 | 288 | 1.694* |
| GGBY-Yb0.5 | 728 | 897 | 169 | 4.95 | - | - |
| GGBY-Yb3 | 730 | 902 | 172 | 5.10 | 294 | 1.778** |
| GGB-Yb7 | 730 | 886 | 156 | 5.35 | 293 | 1.778** |

*972 nm **935 nm

A shift towards higher temperatures of the glass transition temperature, from 675°C to 708°C, and of the onset of crystallization temperature, from 840°C to 876°C, with the insertion of ytterbium oxide in GGBK-Yb0 matrix is noticeable. On the other hand, the substitution of potassium by yttrium in the glass results in further increase of $T_g$. The joint increase of both $T_g$ and $T_x$ can be directly correlated with the strengthening of the glass network with the insertion of $Yb^{3+}$ ions. This result is unusual as it is well-known that insertion of rare-earth (RE) ions in glassy networks, generally acting as nucleating agent [25], results in a decrease of their thermal stability vs temperature. Here one can assume that the $Yb^{3+}$ ions are not only easily dissolved into the vitreous network but that they are also incorporated (at least partly) into the glass back-bone, contributing to its reinforcement and thus increasing its $T_g$ and $T_x$.

The thermal stability criterion $\Delta T = T_x - T_g$ measured on the ytterbium-containing glasses is relatively high, where values range between 151 °C and 172 °C. This result is not expected as it is known that addition of RE ions like $Yb^{3+}$ into a glassy material tends to decrease its stability vs crystallization [25]. Furthermore, although it is admitted that a large $\Delta T$ indicates a strong potential for thermal shaping and fiber drawing, it was only partially confirmed by the experiment on the glass $28Ga_2O_3 – 37GeO_2 – 23BaO – 12K_2O$ [23]. Further investigation is required to understand the structural role played by $Yb^{3+}$ in such glasses.

One can notice in Table 2 that the density of the GGBK-Yb*x* glasses also increases with the addition of ytterbium oxide and is much higher in the yttrium-containing glasses (4.95 $g.cm^{-3}$ to 5.10 $g.cm^{-3}$) than the potassium-containing ones (4.30 $g.cm^{-3}$ to 4.54 $g.cm^{-3}$). This can be easily explained by the higher density of $Yb_2O_3$ and $Y_2O_3$ ($\rho_{Yb2O3}$ = 9.17 $g.cm^{-3}$ and $\rho_{Y2O3}$ = 5.01 $g.cm^{-3}$) compared to the other constituents of the glass. The short wavelength cut-off $\lambda_{UV}$ of the GGBK-Yb*x* samples shows a red shift with the introduction of ytterbium and/or yttrium oxides (Table 2).

The linear refractive index of the glass samples measured at 935 nm or 972 nm are shown in Table 2. A clear increase of the refractive index with the $Yb_2O_3$ content is observed, which is consistent with the observation made on the samples density reported in Table 2, and are higher in yttrium-containing glasses.

### *3.2. Structural studies*

Unpolarized Raman spectra for the investigated glasses are presented in Figure 2. First, we focus on the vibrational spectra of the potassium germano-gallate matrix (GGBK-Yb0) which can be decomposed into low (200 – 400 $cm^{-1}$), intermediate (400 – 640 $cm^{-1}$) and high frequency regions (640 − 1000 $cm^{-1}$). The low and intermediate frequency envelopes can be attributed mainly to highly coupled bending modes involving ($T^{[4]} – O – T^{[4]}$) bridges with T being either gallium or germanium; the brackets refer to the coordination number of the atoms [20], [22]. The high frequency region contains more localized stretching features of germanium and gallium sites involved respectively in (1) $Q^{n\,=\,1,2,3,4}$ germanate units [20], [26]–[28] where *Q* represents structural units (here tetrahedral ones) and *n* the number of bridging oxygens between two glass former cations (Ge or Ga), and (2) stretching vibrations involving $Q^4$ gallate units [20], [29], [30] in mixed interconnected $Ga^{[4]} – O^- – Ge^{[4]}$ bridges [20]. The negative charge on oxygen ions is balanced by the modifier cations. In our case, $Q = [2BaO + 1KO_{1/2} + 3YbO_{3/2}] / [GaO_{3/2}] > 1$, therefore we expect to see both latter modes.

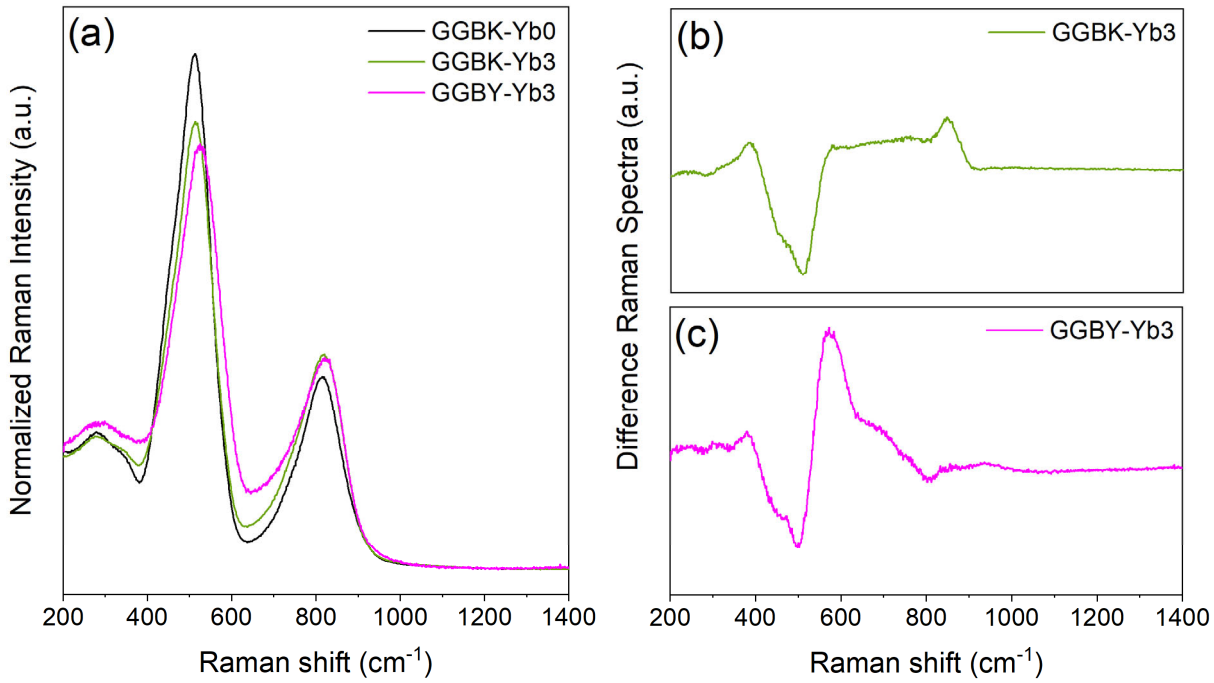


**Figure 2**. (a) Normalized Raman spectra of the GGBK-Yb0, GGBK-Yb3 and GGBY-Yb3 glass samples, (b) effect of $Yb_2O_3$ addition in GGBK-Yb0: difference Raman spectra between GGBK-Yb0 and GGBK-Yb3 and (c) effect of substitution of potassium by yttrium: difference Raman spectra between GGBY-Yb3 and GGBK-Yb3.

Firstly, we turn our focus to the influence of the ytterbium oxide additions to the GGBK-Yb0 glass matrix. We normalized the Raman spectra to the area to observe both evolutions, that of the intermediate region centered at 512 $cm^{-1}$ which is related to the 3D network of gallium and germanium [28] and the high frequency region one. The addition of 3 mol% of $Yb_2O_3$ to the GGBK-Yb0 glass matrix results in a decrease of the band centered at 512 $cm^{-1}$, which is a signature of the modification of the 3D interconnected network. On the other hand, the broad band in the uppermost domain peaking at 817 $cm^{-1}$ increases in intensity with the increase of $Yb_2O_3$ content. Based on the literature [27], this broad band comprises vibrational modes assigned to Non-Bridging Oxygen (NBO) on germanium tetrahedral moieties, particularly to $Q^2$ $(Ge\varnothing_2O_2)^{2-}$ and $Q^3$ $(Ge\varnothing_3O)^-$ entities at ~750 $cm^{-1}$ and ~850 $cm^{-1}$, respectively. The increase of $Yb_2O_3$ induces further increase of these two latter modes and a slight shift of the intermediate broad frequency band. The results are provided in Figures S1 (Supporting Information). In order to visualize better the effect of ytterbium addition in the GGBK-Yb0 glass matrix, we did the Raman difference between GGBK-Yb0 and GGBK-Yb3 and the spectrum is shown in Figure 2(b). We clearly see a broad band at ~750 $cm^{-1}$ and another at ~850 $cm^{-1}$ related to NBO units.

Secondly, we want to focus on the substitution of potassium by yttrium ions. In the uppermost part, we observe similar spectra for both GGBK-Yb3 and GGBY-Yb3, with no change in the intensity of the band at ~817 $cm^{-1}$ related to NBO. However, the intermediate frequency band is affected in intensity

and shows a slight blue shift. The difference Raman spectra between GGBY-Yb3 and GGBK-Yb3 is shown in Figure 2c. It certainly shows that the NBOs vibrations are less influenced by this substitution. We definitely see a new vibrational band at ~700 $cm^{-1}$. Another feature that we remark is a signal at 575 $cm^{-1}$ and a more pronounced negative shift at 500 $cm^{-1}$ in the Y-containing glass compared to the K-containing ones. All these observations together with the modifications in the low frequency domain indicate that the germano-gallate glass former network units are affected by the change of the nature of charge compensation [31].

### *3.3. Absorption and emission cross-sections*

The absorption cross-section of the studied $Yb^{3+}$-containing samples can be obtained from the recorded absorption coefficient spectra and the $Yb^{3+}$ ionic density (see Table 1). The absorption cross-section spectra in the NIR range of the doped samples are illustrated in Figure 3a. The samples present an absorption peak centered at the $^2F_{7/2} \rightarrow {}^2F_{5/2}$ transition (976 nm). The emission cross-section of the glass samples can be then evaluated using the Fuchbauer-Ladenburg equation [32]:

$$\sigma_{em}(\lambda) = \frac{\lambda^4 \, Ar \, g(\lambda)}{8\pi n^2 c}, \tag{1}$$

$$g(\lambda) = \frac{\int I(\lambda) d\lambda}{I_{max}}, \tag{2}$$

$$Ar = \frac{8\pi c n^2 \, (2J' + 1)}{\lambda_p^4 (2J + 1)\rho} \int \alpha(\lambda) d\lambda \,, \tag{3}$$

Where $Ar$ is the spontaneous emission probability, $c$ the velocity of light, $n$ the refractive index, $\lambda_p$ the absorption peak wavelength (976 nm), $\rho$ the $Yb^{3+}$ concentration density, $\alpha(\lambda)$ the absorption coefficient, $J$ and $J'$ the total momentum for the upper and lower levels and $g(\lambda)$ the normalized line shape function of the NIR emission of $Yb^{3+}$. The spectroscopic properties, $\sigma_{abs}$ and $\sigma_{em}$, have been evaluated and are shown in Table 3.

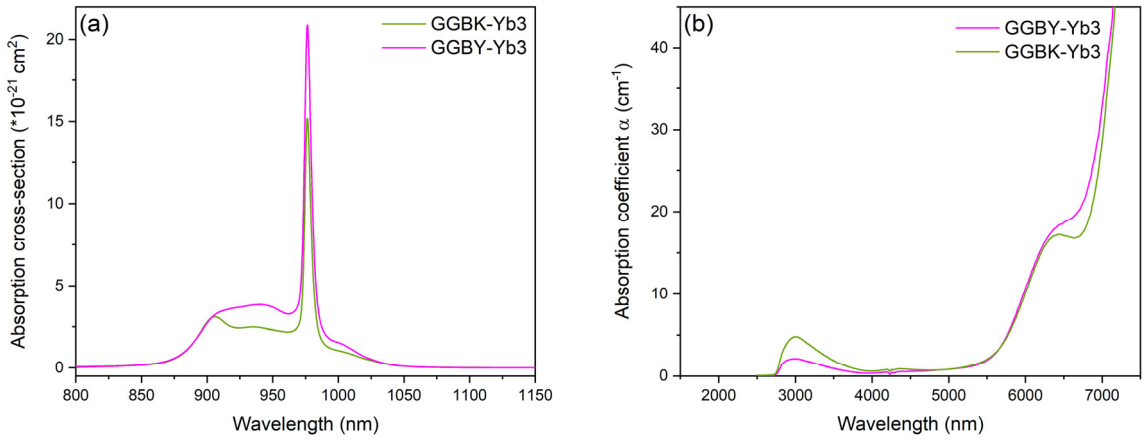


**Figure 3**. (a) Absorption cross-section spectra in the NIR region and (b) absorption coefficient spectra of the samples GGBK-Yb3 and GGBY-Yb3 in the mid-IR region.

Figure 3b shows the absorption coefficient measurements in the mid-IR region with an optical transparency extending up to 5.5 µm. One can see two absorption bands at 3000 nm and 4200 nm. They are related to hydroxyl (OH) vibrations due to the absence of dehydration steps during the glass synthesis. Regarding the IR-multiphonon cut-off, it constitutes a band at ~6200 nm which could be an overtone related to NBO on $GeO_4$ units located at 800 $cm^{-1}$ [20], and a absorption edge at ~7000 nm.

### *3.4. Photoluminescence*

The luminescence properties were collected for all the samples in powder. The photoluminescence excitation spectra are shown in Figure 4a. By monitoring the emission at 976 nm, a broad excitation band centered at 255 nm for GGBK-Yb3 and 266 nm for GGBY-Yb3 is observed. The photoluminescence emission spectra recorded under excitation at 265 nm are presented in Figure 4b. A broad emission from 950 nm to 1100 nm is observed, characteristic of the emission spectrum of $Yb^{3+}$ ions in a glass. These emissions correspond to the splitting of the electronic transition $^2F_{5/2}$ to $^2F_{7/2}$ due to the breaking of 4f level degeneracy. One can see that the intensity of the 976 nm peak is higher in GGBY-Yb3 than GGBK-Yb3. Moreover, one can also notice that there is a difference of lineshape in particular above 980 nm indicating a difference of the ytterbium environment. Additionally, it is worth to note that a strong quenching effect for ytterbium content above 1 mol% of $Yb_2O_3$ is observed in GGBK-Yb*x* series which traduces a clustering of $Yb^{3+}$ ions (see Figure S2 in supporting information).

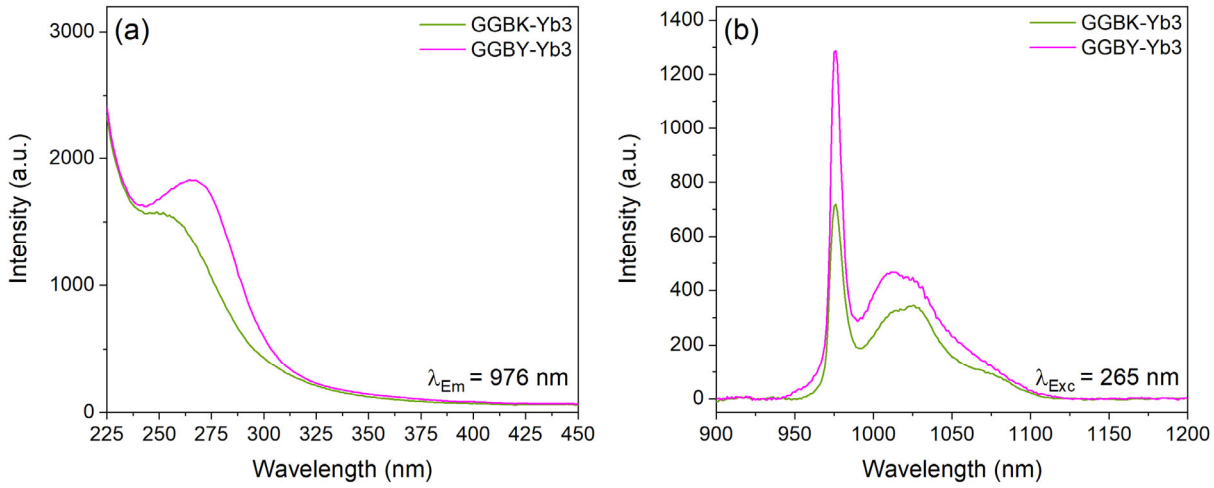


**Figure 4.** (a) Excitation spectra for $\lambda_{Em}$ = 976 nm and (b) emission spectra for $\lambda_{Exc}$ = 265 nm of the GGBK-Yb3 and GGBY-Yb3 glasses.

### *3.5. Laser performance parameters*

Different parameters related to the laser performance can be then calculated from the absorption and emission cross-sections spectra. In the case of $Yb^{3+}$ doped materials a significant ground-state absorption at the laser wavelength may occur, even if it could be considered as quasi-four level systems. First, $\beta_{min}$, which is defined as the minimum fraction of $Yb^{3+}$ ions that must be excited to balance the gain with the ground-state absorption at laser wavelength (extraction wavelength) $\lambda_{ext}$ is given by [33]:

$$\beta_{min} = \frac{\sigma_{abs}(\lambda_{ext})}{\sigma_{abs}(\lambda_{ext}) + \sigma_{em}(\lambda_{ext})} \quad (4)$$

The smaller $\beta_{min}$ is, the lower the resonant absorption losses are at the $\lambda_{ext}$ wavelength. The pump saturation intensity, $I_{sat}$, is also an important laser parameter and can be obtained using [33]:

$$I_{sat} = \frac{hc}{\lambda_{pump} \cdot \sigma_{abs}(\lambda_{pump}) \cdot \tau_{exp}} \quad (5)$$

where $\frac{hc}{\lambda_{pump}}$ is the pumping energy and $\tau_{exp}$ is the experimental emission lifetime.

Finally, $I_{min}$ is a parameter which evaluates the minimum absorbed pump intensity. This parameter represents the threshold to be reached for obtaining gain. $I_{min}$ takes into account both the absorption and emission properties and is calculated by the following expression [33]:

$$I_{min} = \beta_{min} I_{sat} \quad (6)$$

**Table 3.** Spectroscopic properties and laser performance parameters of $Yb^{3+}$-containing glasses.

| Sample | $\sigma_{abs}$ (976nm) ($10^{-21}$ cm$^2$) | $\sigma_{em}$ (1010 nm) ($10^{-21}$ cm$^2$) | $\sigma_{em}$ (1060 nm) ($10^{-21}$ cm$^2$) | $\beta_{min}$ (1010 nm) | $\beta_{min}$ (1060 nm) | $I_{sat}$ (kW/cm$^2$) | $I_{min}$ (1010 nm) (kW/cm$^2$) | $I_{min}$ (1060 nm) (kW/cm$^2$) |
|---|---|---|---|---|---|---|---|---|
| GGBK-Yb3 | 15.10 | 3.20 | 1.45 | 0.207 | 0.042 | 37.466 | 7.78 | 1.60 |
| GGBY-Yb3 | 20.84 | 4.89 | 2.33 | 0.190 | 0.025 | 18.054 | 3.43 | 0.45 |

In order to evaluate the potential lasing performance of the samples in diode-laser pump systems, we determined the values of $\beta_{min}$, $I_{sat}$ as well as $I_{min}$ for two wavelengths of emission at 1010 nm and 1060 nm and the results are shown in Table 3. The $I_{min}$ values obtained are comparable to values reported for lead germanate glass with $I_{min}$ equals to 2.8 kW/cm$^2$ for $\lambda_{ext}$ = 1009 nm [34]. We have found lower values of $\beta_{min}$, $I_{sat}$ and $I_{min}$ in GGBY-Yb3 compared to GGBK-Yb3 glass at both wavelengths 1010 nm and 1060 nm, making the GGBY-Yb3 glass most promising since for laser materials, the pump saturation intensity should be low in order to minimize the pumping intensity.

### *3.6. Lifetime studies*

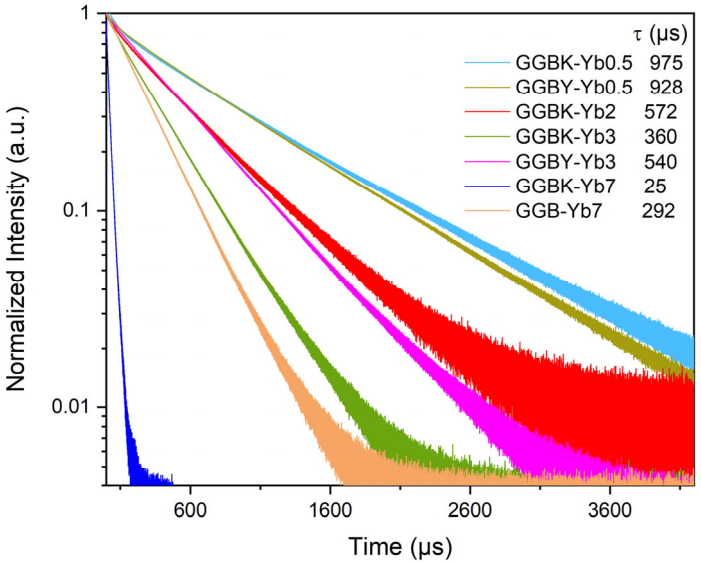


**Figure 5.** Normalized decay curves for the $Yb^{3+}$: $^2F_{5/2} \rightarrow {}^2F_{7/2}$ transition of the germano-gallate glasses as a function of $Yb^{3+}$ concentration, under laser excitation at 940 nm.

The luminescence decay curves of the $Yb^{3+}$: $^2F_{5/2} \rightarrow {}^2F_{7/2}$ transition were measured for an excitation at 940 nm and for emission at 1040 nm. Figure 5 shows the normalized decay curves for different $Yb^{3+}$ concentrations in GGBK-Yb and GGBY-Yb glass samples. If one considers a single $Yb^{3+}$environment and isolated sites in the $^2F_{5/2}$ metastable state, the luminescence decay is expected monoexponential with a single time constant τ. Indeed, all the decay curves could be fitted with a single exponent except the

GGBK-Yb7 where a second short decay could be noticed (for GGBK-Yb7, we chose the average lifetime). As the ytterbium oxide content increases from 0.5% to 7%, the lifetime τ of the $Yb^{3+}$:$^2F_{5/2}$ excited state shortens from 0.975 ms (GGBK-Yb0.5) to 0.025 ms (GGBK-Yb7) in GGBK-Yb, and from 0.928 ms (GGBY-Yb0.5) to 0.292 ms (GGB-Yb7) in GGBY-Yb. This decrease is related to concentration quenching effect. The shortening of lifetime due to the quenching effect could be either due to multiphonon relaxation, energy transfer among $Yb^{3+}$ ions or direct coupling with $OH^-$ groups. The $OH^-$ groups lead to a broad absorption band around 3000 nm in germano-gallate glasses as is shown in Figure 3b. In these glasses, the amount of $OH^-$ groups is expected to be low (around 90-230 ppm quantified from the absorption coefficient spectra), thus it can be assumed that the most dominant mechanism for lifetime quenching is the energy transfer among $Yb^{3+}$ ions leading to energy migration followed by non-radiative transfer. The longest lifetime measured is 0.975 ms for GGBK-Yb0.5 and 0.928 ms for GGBY-Yb0.5, which are comparable to that reported for the $Yb^{3+}$:YAG crystal (1.1 ms for a concentration of 2.5 at.% $Yb^{3+}$) [16] and lead germanates [34], gallo-germanates (0.94 ms for 1 mol% $Yb^{3+}$) [15] and other kinds of oxide glasses [35], but shorter than that measured for an oxyfluoride glass based on heavy metals and silicates (1.52 ms for a concentration of 2 mol% $Yb^{3+}$) [25]. Our value is in accordance with the high refractive index of germano-gallates which contributes to rise the radiative cross section and indeed lower the emission lifetime.

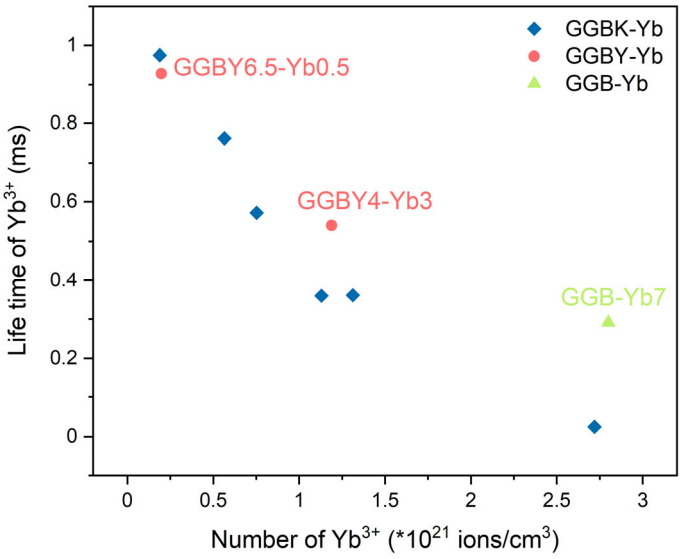


**Figure 6.** NIR lifetime of $Yb^{3+}$ vs number of $Yb^{3+}$ ions in GGBK-Yb, GGBY-Yb and GGB-Yb.

Figure 6 presents the lifetime values for NIR signals as a function of the number of the volumic amount of $Yb^{3+}$ ions. The lifetime decreases with increasing the number of $Yb^{3+}$ ions in the glass. The lifetime shortening is attributed to the ytterbium clustering effect which tends to promote energy migration and non-radiative transfer [8]. This plot allows to view better the slope of the decreasing trend of the lifetime between GGBK-Yb and GGBY-Yb, which seems to be faster in the former. Moreover, glasses containing $Y^{3+}$ possess higher lifetime than $K^+$-containing glasses. This should be related to a rare earth

clustering effect in GGBK-Yb3 glass. According to time-resolved spectroscopy, the incorporation of $Y^{3+}$ in the glass matrix present advantages over the $K^{+}$ counterpart for homogeneous distribution of $Yb^{3+}$ ions in the glass matrix.

### *3.7. Fiber drawing and optical losses*

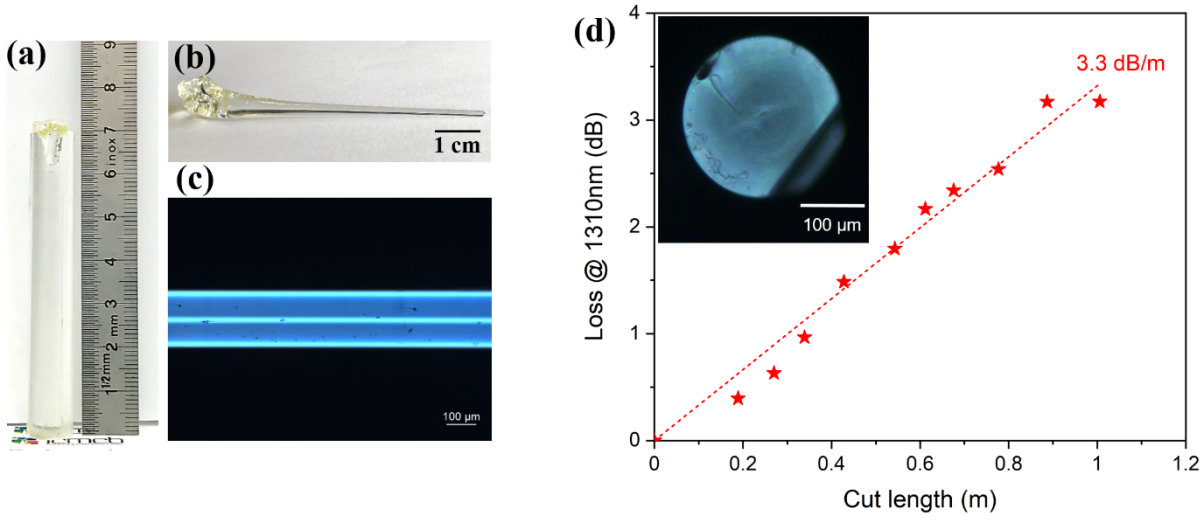


**Figure 7.** Preform-based optical fiber manufacturing for GGBY-Yb3 glass (a) Photograph of macroscopic GGBY-Yb3 glass preform prior to drawing (b) glass drop (c) microscope image of the fiber and (d) loss measurements (inset: fiber cross-sectional view).

We now demonstrate the suitability for drawing of yttrium-containing active rare-earth doped glass medium. The results provide insights and practical steps in the shaping ability of these glasses of technological interest into optical fibers. It was reported that the introduction of yttrium oxide in germano-gallate glasses enables to implement the preform drawing technology [23].

In this work, the $29.6Ga_2O_3 – 39.1GeO_2 – 24.3BaO – 4Y_2O_3 – 3Yb_2O_3$ (GGBY-Yb3) glass composition was chosen for the fiber drawing process. This glass presents a high thermal stability parameter ($\Delta T$ = 172 °C) against devitrification, which can ensure the obtainment of transparent fibers free from crystalline inclusions. Mono-index preforms of GGBY-Yb3 glass composition were successfully drawn into tens of meters long fibers with diameters ranging between 200-250 µm. Figure 7 shows a photograph of the GGBY-Yb3 glass preform prior to drawing, a glass drop and a longitudinal microscopic image of the fiber (panels (a), (b) and (c) respectively). In order to confirm the optical transparency of the fibers, attenuation measurements were performed by the cut-back method at the wavelengths of 1310 nm on initial sections of 2 meters (Fig. 7d). We measured optical attenuations of 3.3 dB/m for the GGBY-Yb3 glass. This value is well expected due to the fact that mono-index preforms were elaborated where the surrounding conditions could greatly affect such measurement.

## 4. Conclusion

The physicochemical, optical, structural and photoluminescent properties of the germano-gallate glasses following the composition laws: (100-$x$) ($28Ga_2O_3 – 37GeO_2 – 23BaO – 12K_2O$) – $xYb_2O_3$ ($x$ = 0, 0.5 and 3 mol.%) as well as $29.6Ga_2O_3 – 39.1GeO_2 – 24.3BaO – 7$ ($yY_2O_3 – zYb_2O_3$) ($y$ = 6.5, 4, 0 and $z$ = 0.5, 3, 7 mol% respectively) have been investigated. The obtained glasses present a wide transparency window from approximately 280 nm up to 5.5 µm. When the ytterbium oxide content is increased, the glass transition temperature and density increase, as well as the linear refractive index. Raman spectroscopy demonstrates on one hand that ytterbium additions depolymerize the 3D germano-gallate network. On the other hand, potassium substitutions by yttrium result in modifications in the 3D glass network by affecting the gallate units via the change in the charge compensation nature. The lifetime of $^2F_{5/2}$ level shortens from 0.975 ms to 0.025 ms in GGBK-Yb glasses and from 0.928 ms to 0.292 ms in GGBY-Yb glasses with increasing $Yb^{3+}$ concentration but remains higher in the latter system at higher concentrations due to probably better homogenization of $Yb^{3+}$ ions in the glass matrix. Laser performance parameters were compared, and that GGBY-Yb3 glass possesses higher figure of merit. GGBY-Yb3 glass preform was shaped into crystal-free, lighting guide fibers by conventional preform pulling with optical losses of about 3.3 dB/m at 1310 nm on unpurified, mono-index fibers. The results of $Yb^{3+}$-doped yttrium-containing glasses indicate their high potential to be used as NIR optical gain medium.

## Acknowledgements

This research was supported by Agence Nationale de la Recherche (ANR) (ANR Grant ANR-18-CE08-0004-02), the CPER Campus B, and the New Aquitaine region. This project has received funding from the European Union's Horizon 2020 research and innovation program under the Marie-Skłodowska-Curie grant agreement N°823941 (FUNGLASS). This research was also supported by the Canadian Excellence Research Chair program (CERC) in Photonics Innovations and the Aquitaine Region. The authors are also grateful to the Natural Sciences and Engineering Research Council of Canada (NSERC), the Fonds de Recherche Québecois sur la Nature et les Technologies (FRQNT) and the Canadian Foundation for Innovation (CFI) for the financial support. Mobilities were supported by the LIA LuMAQ (CNRS) and the Agence Nationale de la Recherche (ANR) with the program "Investissement d'avenir" number ANR-10-IDEX-03-02.

## References

[1] D. J. Richardson, J. Nilsson, and W. A. Clarkson, "High power fiber lasers: current status and future perspectives [Invited]," *J. Opt. Soc. Am. B, JOSAB*, vol. 27, no. 11, pp. B63–B92, Nov. 2010, doi: 10.1364/JOSAB.27.000B63.

[2] C. Hönninger *et al.*, "Ultrafast ytterbium-doped bulk lasers and laser amplifiers," *Applied Physics B*, vol. 69, pp. 3–17, Jul. 1999, doi: 10.1007/s003400050762.

[3] B. I. Galagan *et al.*, "Erbium-ytterbium codoped phosphate core/double silica clad composite optical fibres for compact amplifiers," *Quantum Electronics*, vol. 48, pp. 550–553, Jun. 2018, doi: 10.1070/QEL16633.

[4] Y. Zaouter *et al.*, "47-fs diode-pumped $Yb^{3+}$:$CaGdAlO_4$ laser," *Opt. Lett., OL*, vol. 31, no. 1, pp. 119–121, Jan. 2006, doi: 10.1364/OL.31.000119.

[5] A. Brenier *et al.*, "Growth and spectroscopic properties of $Yb^{3+}$-doped $Li_6Y(BO_3)_3$ single crystal," *Journal of Luminescence*, vol. 126, pp. 547–550, Oct. 2007, doi: 10.1016/j.jlumin.2006.08.101.

[6] M. Delaigue, V. Jubera, J. Sablayrolles, J. P. Chaminade, A. Garcia, and I. Manek-Hönninger, "Mode-locked and Q-switched laser operation of the Yb-doped $Li_6Y(BO_3)_3$ crystal," *Applied Physics B*, vol. 87, pp. 693–696, Jan. 2007, doi: 10.1007/s00340-007-2641-7.

[7] H. Dong *et al.*, "Effect of co-dopants on the spectral property of $Yb^{3+}$ doped silica glasses at 1018 nm," *Optical Materials*, p. 111761, Nov. 2021, doi: 10.1016/j.optmat.2021.111761.

[8] A. S. Pinheiro *et al.*, "Laser performance parameters of $Yb^{3+}$ doped UV-transparent phosphate glasses," *Chemical Physics Letters*, vol. 592, pp. 164–169, Jan. 2014, doi: 10.1016/j.cplett.2013.12.022.

[9] M. Hongisto, A. Veber, N. G. Boetti, S. Danto, V. Jubera, and L. Petit, "Transparent $Yb^{3+}$ doped phosphate glass-ceramics," *Ceramics International*, vol. 46, no. 16, Part B, pp. 26317–26325, Nov. 2020, doi: 10.1016/j.ceramint.2020.01.121.

[10] L. Zhang, Y. Xia, X. Shen, and W. Wei, "Effects of $GeO_2$ concentration on the absorption and fluorescence behaviors of $Yb^{3+}$ in tellurite glasses," *Journal of Luminescence*, vol. 198, Feb. 2018, doi: 10.1016/j.jlumin.2018.02.024.

[11] V. Jubera, J. Sablayrolles, F. Guillen, R. Decourt, M. Couzi, and A. Garcia, "From the infrared to the visible range: Spectroscopic studies of ytterbium doped oxyborates," *Optics Communications*, vol. 282, no. 1, pp. 53–59, Jan. 2009, doi: 10.1016/j.optcom.2008.09.075.

[12] C. Jiang, J. Zhang, P. Deng, G. Huang, H. Mao, and F. Gan, "Optimization of spectroscopic properties of ytterbium-doped laser glasses," *Sci. China Ser. E-Technol. Sci.*, vol. 42, no. 6, pp. 616–622, Dec. 1999, doi: 10.1007/BF02916998.

[13] L. C. Courrol *et al.*, "Study of the most suitable new glass laser to incorporate ytterbium: alkali niobium tellurite, lead fluorborate or heavy metal oxide," *Journal of Luminescence*, vol. 102–103, pp. 106–111, May 2003, doi: 10.1016/S0022-2313(02)00475-1.

[14] B. Peng, L. Jiang, X. Qiu, Z. C. Fan, and W. Huang, "Ytterbium doped heavy metal oxide glasses with high emission cross-section," *Journal of Alloys and Compounds*, vol. 398, pp. 170–172, Aug. 2005, doi: 10.1016/j.jallcom.2005.01.005.

[15] L. Zhang, Y. Xia, X. Shen, R. Yang, and W. Wei, "Investigations on the effects of the Stark splitting on the fluorescence behaviors in $Yb^{3+}$-doped silicate, tellurite, germanate, and phosphate glasses," *Optical Materials*, vol. 75, pp. 1–6, Jan. 2018, doi: 10.1016/j.optmat.2017.10.008.

[16] J. Dong, M. Bass, Y. Mao, P. Deng, and F. Gan, "Dependence of the $Yb^{3+}$ emission cross section and lifetime on temperature and concentration in yttrium aluminum garnet," *J. Opt. Soc. Am. B, JOSAB*, vol. 20, no. 9, pp. 1975–1979, Sep. 2003, doi: 10.1364/JOSAB.20.001975.

[17] R. Stepien, M. Franczyk, D. Pysz, I. Kujawa, M. Klimczak, and R. Buczynski, "Ytterbium-Phosphate Glass for Microstructured Fiber Laser," *Materials*, vol. 7, pp. 4723–4738, Jun. 2014, doi: 10.3390/ma7064723.

[18] M. Franczyk *et al.*, "High efficiency $Yb^{3+}$-doped phosphate single-mode fibre laser," *Laser Phys. Lett.*, vol. 14, no. 10, p. 105102, Sep. 2017, doi: 10.1088/1612-202X/aa7d39.

[19] S. S. Bayya, G. D. Chin, J. S. Sanghera, and I. D. Aggarwal, "Germanate glass as a window for high energy laser systems," *Opt. Express, OE*, vol. 14, no. 24, pp. 11687–11693, Nov. 2006, doi: 10.1364/OE.14.011687.

[20] T. Skopak *et al.*, "Structure and Properties of Gallium-Rich Sodium Germano-Gallate Glasses," *J. Phys. Chem. C*, vol. 123, no. 2, pp. 1370–1378, Jan. 2019, doi: 10.1021/acs.jpcc.8b08632.

[21] T. Skopak *et al.*, "Structure-properties relationship study in niobium oxide containing $GaO_{3/2}$-$LaO_{3/2}$-$KO_{1/2}$ gallate glasses," *Materials Research Bulletin*, vol. 112, pp. 124–131, Apr. 2019, doi: 10.1016/j.materresbull.2018.12.007.

[22] T. Skopak *et al.*, "Properties, structure and crystallization study of germano-gallate glasses in the $Ga_2O_3$-$GeO_2$-BaO-$K_2O$ system," *Journal of Non-Crystalline Solids*, vol. 514, pp. 98–107, Jun. 2019, doi: 10.1016/j.jnoncrysol.2019.02.028.

[23] T. Guérineau *et al.*, "Extended germano-gallate fiber drawing domain: from germanates to gallates optical fibers," *Optical Materials Express*, vol. 9, p. 2437, Jun. 2019, doi: 10.1364/OME.9.002437.

[24] F. Calzavara *et al.*, "Glass forming regions, structure and properties of lanthanum barium germanate and gallate glasses," *Journal of Non-Crystalline Solids*, vol. 571, p. 121064, Nov. 2021, doi: 10.1016/j.jnoncrysol.2021.121064.

[25] K. V. Krishnaiah, E. Soares de Lima Filho, Y. Ledemi, G. Nemova, Y. Messaddeq, and R. Kashyap, "Development of ytterbium-doped oxyfluoride glasses for laser cooling applications," *Sci Rep*, vol. 6, no. 1, p. 21905, Feb. 2016, doi: 10.1038/srep21905.

[26] E. I. Kamitsos, Y. D. Yiannopoulos, M. A. Karakassides, G. D. Chryssikos, and H. Jain, "Raman and Infrared Structural Investigation of $xRb_2O\cdot(1-x)GeO_2$ Glasses," *J. Phys. Chem.*, vol. 100, no. 28, pp. 11755–11765, Jan. 1996, doi: 10.1021/jp960434+.

[27] G. S. Henderson, L. G. Soltay, and H. M. Wang, "Q speciation in alkali germanate glasses," *Journal of Non-Crystalline Solids*, vol. 356, no. 44, pp. 2480–2485, Oct. 2010, doi: 10.1016/j.jnoncrysol.2010.03.023.

[28] D. M. McKeown and C. I. Merzbacher, "Raman spectroscopic studies of $BaO$-$Ga_2O_3$-$GeO_2$ glasses," *Journal of Non-Crystalline Solids*, vol. 183, no. 1, pp. 61–72, Apr. 1995, doi: 10.1016/0022-3093(94)00648-2.

[29] L.-G. Hwa, J.-G. Shiau, and S.-P. Szu, "Polarized Raman scattering in lanthanum gallogermanate glasses," *Journal of Non-Crystalline Solids*, vol. 249, no. 1, pp. 55–61, Jul. 1999, doi: 10.1016/S0022-3093(99)00300-2.

[30] L. G. Hwa, Y. R. Chang, and W. C. Chao, "Infrared spectra of lanthanum gallogermanate glasses," *Materials Chemistry and Physics*, vol. 85, no. 1, pp. 158–162, May 2004, doi: 10.1016/j.matchemphys.2003.12.021.

[31] K. Yoshimoto, A. Masuno, M. Ueda, H. Inoue, H. Yamamoto, and T. Kawashima, "Low phonon energies and wideband optical windows of $La_2O_3$-$Ga_2O_3$ glasses prepared using an aerodynamic levitation technique," *Sci Rep*, vol. 7, no. 1, pp. 1–9, Mar. 2017, doi: 10.1038/srep45600.

[32] X. Zou and H. Toratani, "Evaluation of spectroscopic properties of $Yb^{3+}$-doped glasses," *Phys. Rev. B*, vol. 52, no. 22, pp. 15889–15897, Dec. 1995, doi: 10.1103/PhysRevB.52.15889.

[33] L. D. DeLoach, S. A. Payne, L. K. Smith, W. L. Kway, and W. F. Krupke, "Laser and spectroscopic properties of $Sr_5(PO_4)_3F$:Yb," *J. Opt. Soc. Am. B, JOSAB*, vol. 11, no. 2, pp. 269–276, Feb. 1994, doi: 10.1364/JOSAB.11.000269.

[34] V. D. D. Cacho, L. R. P. Kassab, S. L. Oliveira, and P. Verdonck, "Near infrared and blue cooperative emissions in $Yb^{3+}$-doped $GeO_2$–PbO glasses," *Journal of Non-Crystalline Solids*, vol. 352, no. 1, pp. 56–62, Jan. 2006, doi: 10.1016/j.jnoncrysol.2005.11.005.

[35] G. E. Malashkevich *et al.*, "Spectral-luminescent and laser properties of the $(Y_{1-x},Yb_x)_2O_3$−$Al_2O_3$−$B_2O_3$ glasses," *Optical Materials*, vol. 76, pp. 253–259, Feb. 2018, doi: 10.1016/j.optmat.2017.12.042.